Gel-Derived β-Ketoenamine-Linked Tetraisopropylbenzidine-Based Covalent Organic Polymer for High-Performance Symmetric and Asymmetric Supercapacitors

Shubham Kumar[1], Nakul Desai[2], Bharat Z. Dholakiya[1], Sudhakar Y N[*2], and Ritambhara Jangir[*1]

[1]*Department of Chemistry, Sardar Vallabhbhai National Institute of Technology, Ichchanath, Surat-395007, Gujarat, India.*

[2]*Department of Chemistry, Manipal Institute of Technology, Manipal Academy of Higher Education, Manipal 576104, Karnataka, India*

**Correspondence: ritambhara.jangir@chem.svnit.ac.in*

S1. Chemicals and Materials. 2,6-diisopropylaniline, 2,4,6-triformylphloroglucinol, bromine, dodecyltrimethylammonium bromide and iron powder were procured from Sigma-Aldrich, while sodium hydroxide, 1,4-dioxane, THF and acetone were obtained from Spectrochem. Sodium formiate, Pd/C, acetic acid, diethyl ether, NaOH, DMF, anhydrous sodium sulfate, pentane and magnesium sulfate were purchased from Merck. All reagents and solvents were of analytical grade and used without further purification. Freshly prepared deionized water from a Millipore system was employed in all experiments.

S2. Instrumentation. ^{1}H and ^{13}C NMR NMR spectra were obtained using a JEOL ECS 400 MHz spectrometer with DMSO-d_6 and $CDCl_3$ as solvents, and tetramethylsilane (TMS) served as the external reference. Chemical shifts are stated in parts per million (ppm). Fourier-transform infrared (FT-IR) spectra were recorded on a SHIMADZU IR Affinity-1 spectrometer, with 45 scans collected at a 4 cm^{-1} resolution. Solid-state ^{13}C NMR measurements were performed at IISc Bangalore using a JEOL ECX400 MHz spectrometer

equipped with a Bruker magic-angle spinning (MAS) probe. A total of 32,000 scans were conducted to achieve an adequate signal-to-noise ratio. X-ray diffraction (XRD) analysis was carried out using a Panalytical X'Pert Pro diffractometer, and the resulting data were processed with the Reflex module of Materials Studio V6.0. Thermal stability was evaluated using a TGA-DTA TA Module Q600 system. Samples were heated from room temperature (RT) to 800 °C at a heating rate of 10 °C/min under a continuous nitrogen flow of 20 mL/min (combining purge and protective gases). Surface area and porosity measurements were conducted using a Nova Touch LX2 gas sorption analyzer (Quantachrome). Nitrogen adsorption isotherms were recorded at 77 K with ultrahigh-purity N_2 gas at pressure (up to ~1 atm). Field-emission scanning electron microscopy (FE-SEM) and energy-dispersive X-ray spectroscopy (EDX) analyses were performed on a Nova Nano FE-SEM 450 microscope (FEI) after sputter-coating the samples with a platinum layer for 100 seconds to enhance conductivity. Transmission electron microscopy (TEM) and selected area electron diffraction (SAED) were carried out using a Tecnai G2 20 S-TWIN transmission electron microscope (FEI) operating at an accelerating voltage of 200 kV.

S3. Experimental Section

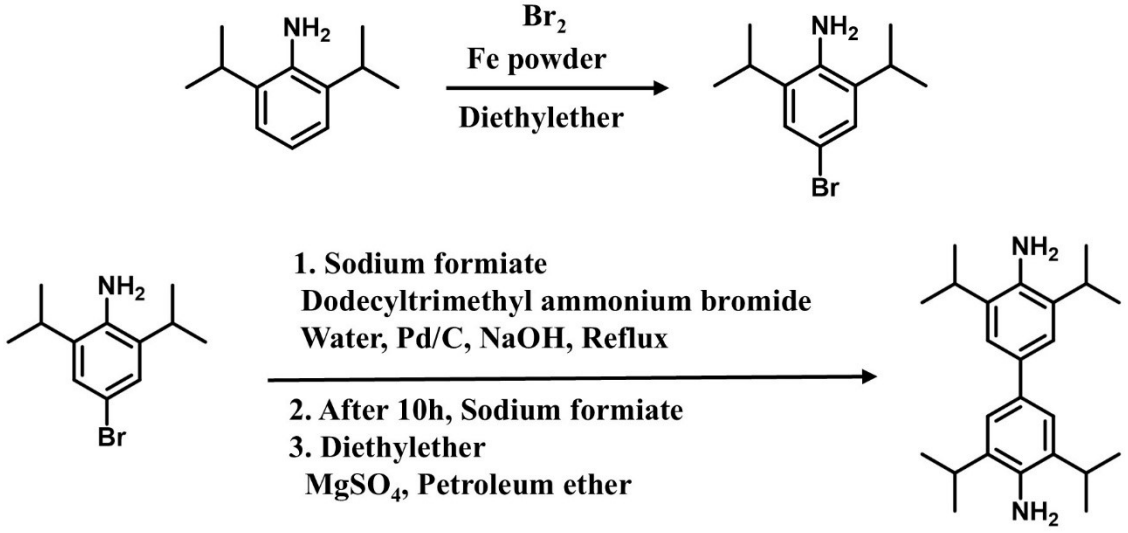

Scheme S1. Synthesis of 2,2′,6,6′-Tetraisopropylbenzidine (TBZ) using 4-bromo,2,6-diisopropylaniline.

S3.1. Synthesis of 4-bromo,2,6-diisopropylaniline. 4-bromo,2,6-diisopropylaniline was synthesized according to a previously reported procedure.[1] Bromine (15 g, 0.094 mol) was added dropwise over a period of 2 hours to a stirred mixture of 2,6-diisopropylaniline (12 g, 0.102 mol) and iron powder (0.056 g, 1 mmol). Upon completion of the addition, the

resulting precipitate was isolated by filtration and recrystallized from ethanol. The obtained white solid was washed thoroughly with 20% aqueous sodium hydroxide solution, followed by extraction with diethyl ether (100 mL). The organic phase was dried over anhydrous sodium sulfate, and the solvent was removed under reduced pressure to afford the product as a white powder (12.2 g, 61% yield).

S3.2. Synthesis of 2,2′,6,6′-Tetraisopropylbenzidine (TBZ). 2,2′,6,6′ Tetraisopropylbenzidine (TBZ) was synthesized according to a previously reported procedure.[2] Sodium formiate (125 mmol), dodecyltrimethylammonium bromide (1.0 g), palladium on charcoal (0.46 g, 3 wt% Pd), sodium hydroxide (1.8 g), and 2,6-diisopropyl-4-bromoaniline (7.7 g, 30 mmol) were combined in 50 mL of water and refluxed under vigorous stirring while a slow stream of air through the reaction mixture. After 10 hours of reflux, an additional 125 mmol of sodium formate was added, and the reaction was continued under the same conditions for another 20 hours. After cooling to room temperature, 100 mL of diethyl ether was added to the resulting biphasic mixture. The aqueous phase was extracted twice with diethyl ether, and the combined organic extracts were dried over magnesium sulfate. The solvent was removed under reduced pressure to yield a red oil, from which the product gradually crystallized as pale violet crystals. The product was recrystallized from pentane, to afford 1.8 g (5.1 mmol, 34% yield). ^{1}H NMR (400 MHz, $CDCl_3$): δ/ppm 7.19 (s, 4 H), 3.73 (s, 4 H), 2.99 (sep, 4H), 1.32 (d, 24H). ^{13}C NMR (400 MHz, $CDCl_3$): δ/ppm 138.92, 133.19, 132.69, 121.74, 28.18, 22.56.

S3.3. Synthesis of TBZTFPG-COP. A mixture comprising 2,2′,6,6′-Tetraisopropylbenzidine (TBZ) (87.26 mg, 0.2475 mmol), 2,4,6-triformylphloroglucinol (TFPG) (35 mg, 0.165 mmol), 6 M aqueous acetic acid (0.3 mL), and dry 1,4-dioxane (3 mL) was introduced into a borosilicate glass tube. The reaction mixture was sonicated for 10 minutes to obtain a uniform suspension. The sealed tube was then heated at 120 °C for 5 days under solvothermal conditions, resulting in the formation of a covalent organic polymer (COP) gel. To purify the COP, the gel was repeatedly washed with 1,4-dioxane, ethyl acetate, DMF, THF, acetone, and methanol to remove unreacted monomers and residual solvents. Upon air-drying, the gel transformed into a brittle monolithic solid, which was further dried at 90 °C to ensure complete solvent removal. The dried monolith was subsequently ground into a fine yellow powder to yield the final COP material (92 mg). Mp >350 °C. Anal. calcd for $C_{270}H_{186}N_{78}O_{18}$: C, 78.97; H, 8.70; N, 5.76. Found: C, 73.891; H, 8.519; N, 6.52. CP-MAS ^{13}C NMR (500 MHz, 295 K): δ 185.65, 157.57, 142.92, 136.14, 123.44, 106.65, 28.87,

23.56 ppm. FT-IR ; 3390, 2962, 2870, 1666, 1573, 1435, 1388, 1288, 1249, 1095, 1010, 941, 871, 817, 732, 663 and 601 cm^{-1}.

S4. FTIR, ^{1}H NMR, ^{13}C NMR spectrum of 2,2′,6,6′-Tetraisopropylbenzidine (TBZ)

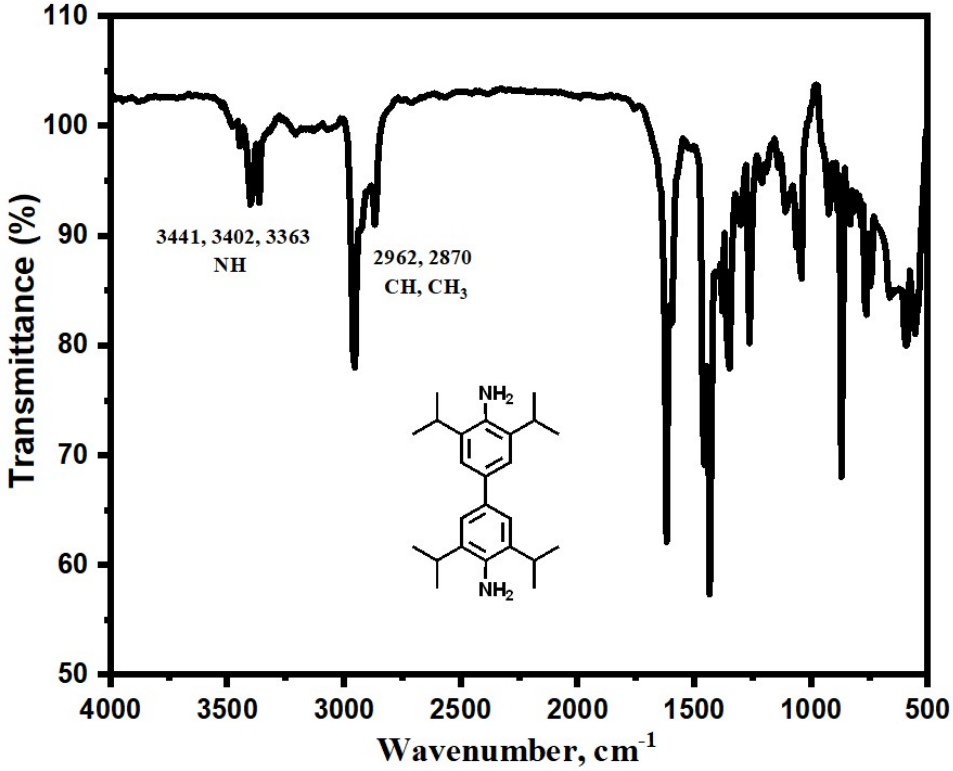

Figure S1. Fourier transform infrared (FT-IR) spectra of 2,2′,6,6′-Tetraisopropylbenzidine (TBZ).

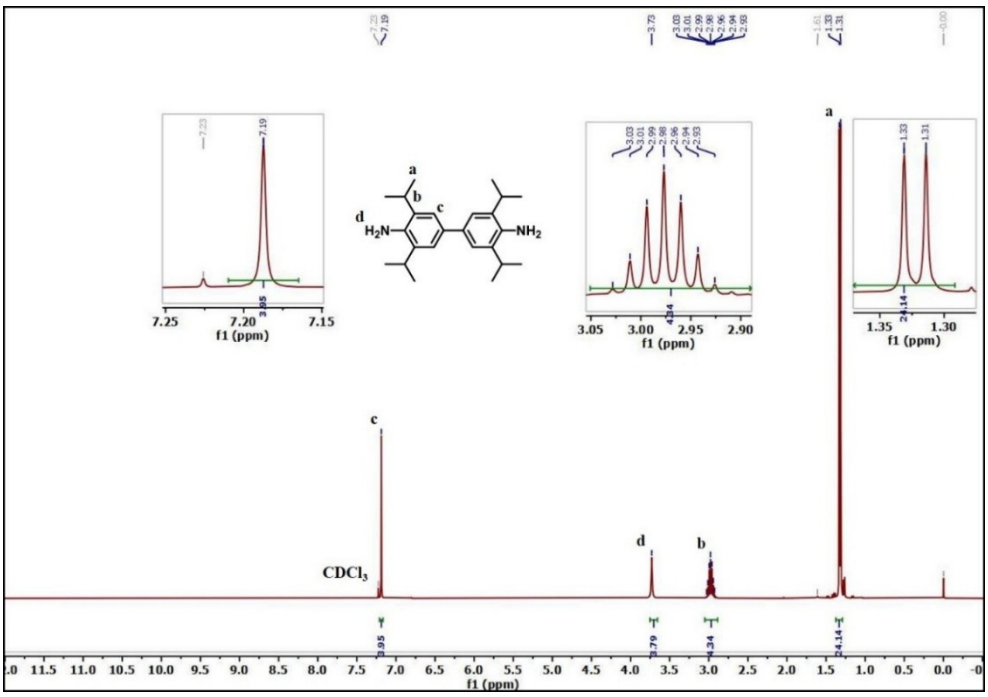

Figure S2. ^{1}H NMR spectrum of TBZ in DMSO-d_6.

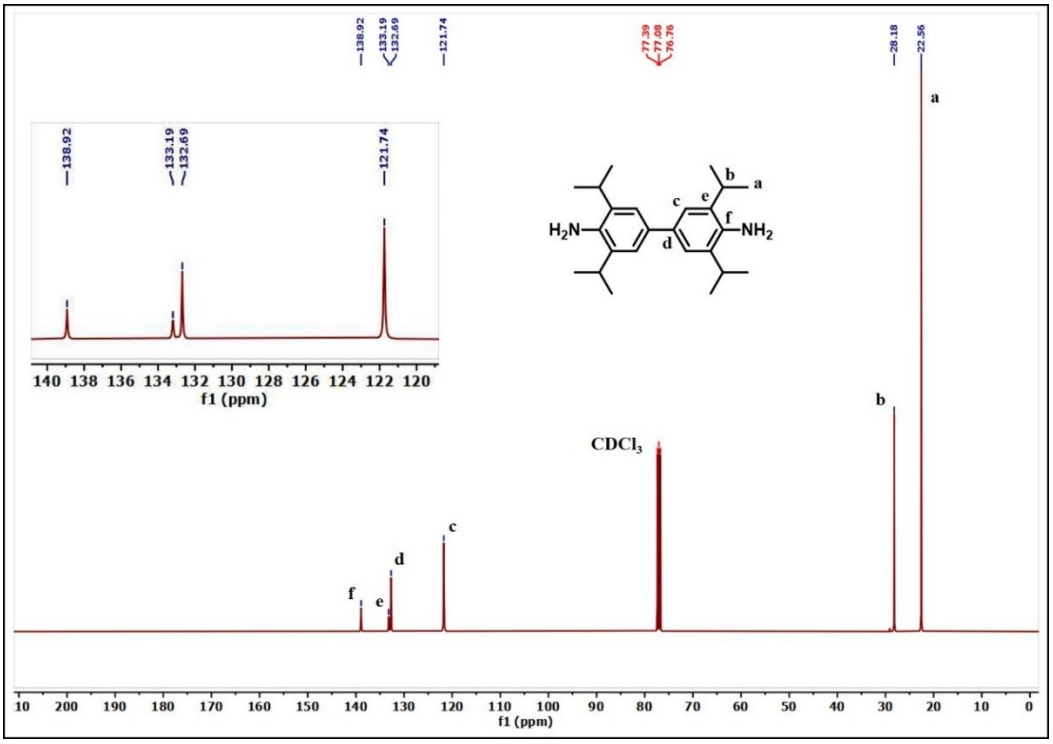

Figure S3. ^{13}C NMR spectrum of TBZ in DMSO-d_6.

S5. CHN, FTIR, TGA, PXRD, FE-SEM and HR-TEM analysis of TBZTFPG-COP

Table S1: CHN analysis of TBZTFPG-COP:

TBZTFPG-COP		**Calculated (Obtained)**		
Mol. Weight (g/mol)	**Formula**	**C%**	**H%**	**N%**
4380.30	$C_{270}H_{186}N_{78}O_{18}$	78.97 (73.891)	8.70 (8.519)	5.76 (6.52)

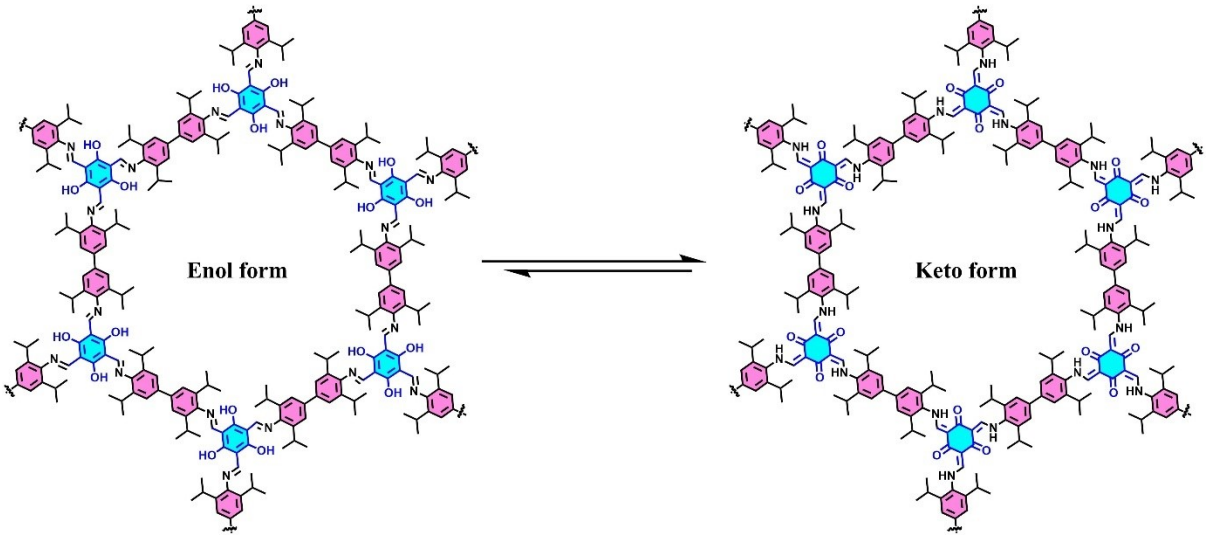

Figure S4. Chemical structure illustrating the tautomerisation of TBZTFPG-COP from the enol-form product to the keto-form product.

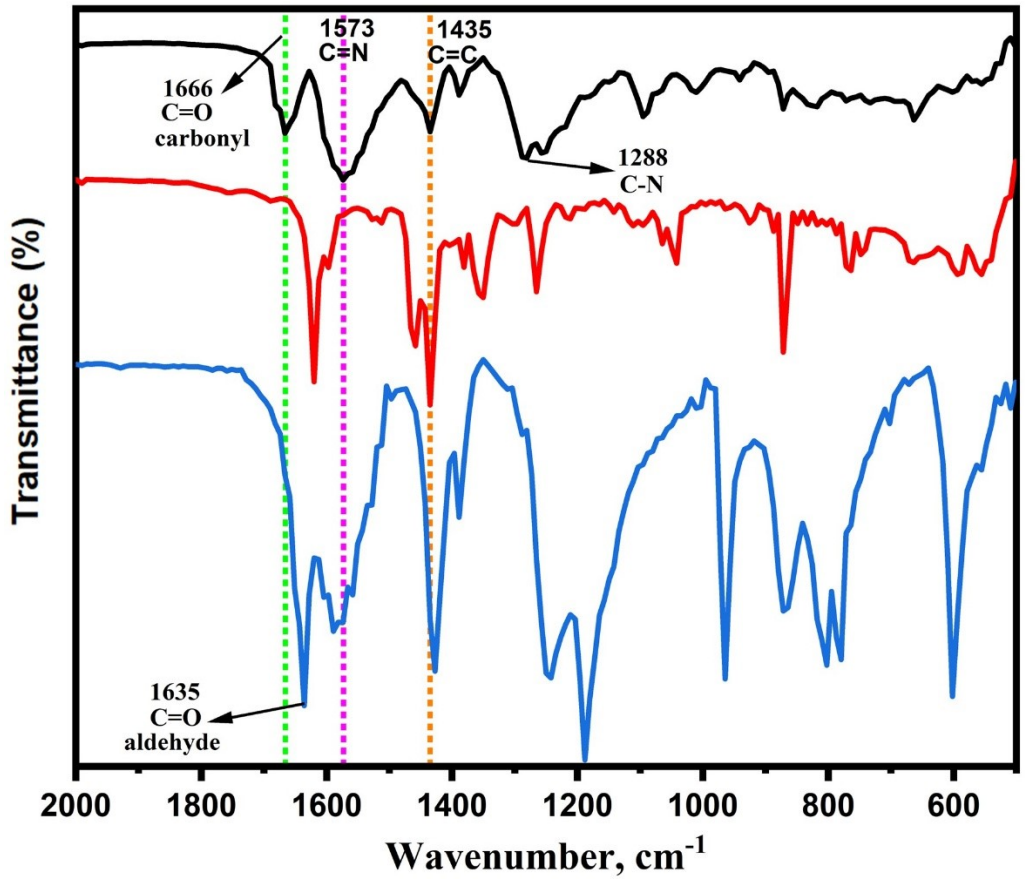

Figure S5. Comparative FT-IR spectra of TBZTFPG-COP and its precursors.

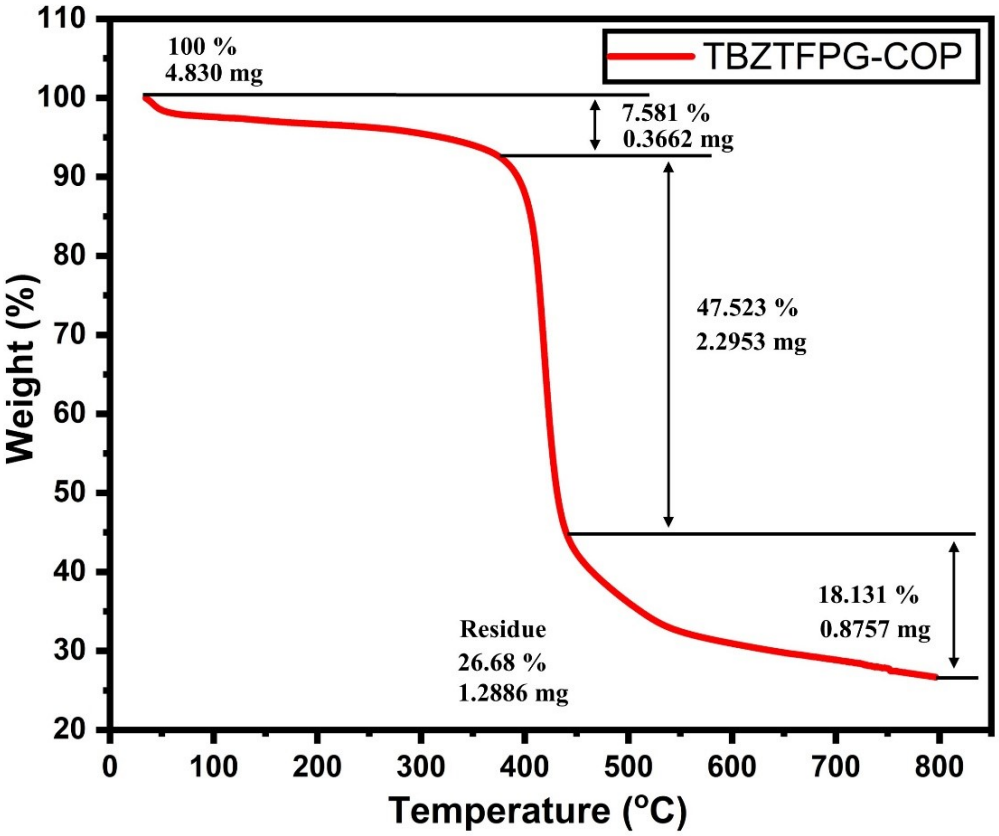

Figure S6. TGA of TBZTFPG-COP under N_2 flow with a heating rate of 10 °C/min.

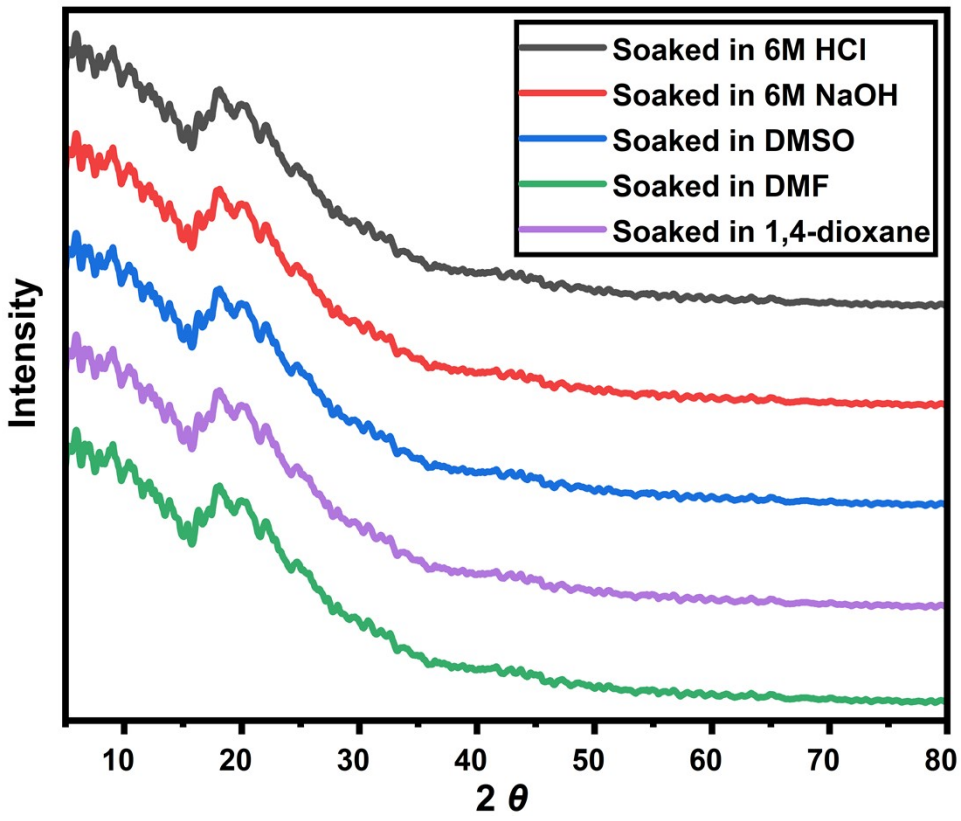

Figure S7. PXRD patterns of TBZTFPG-COP after soaking in different solvents.

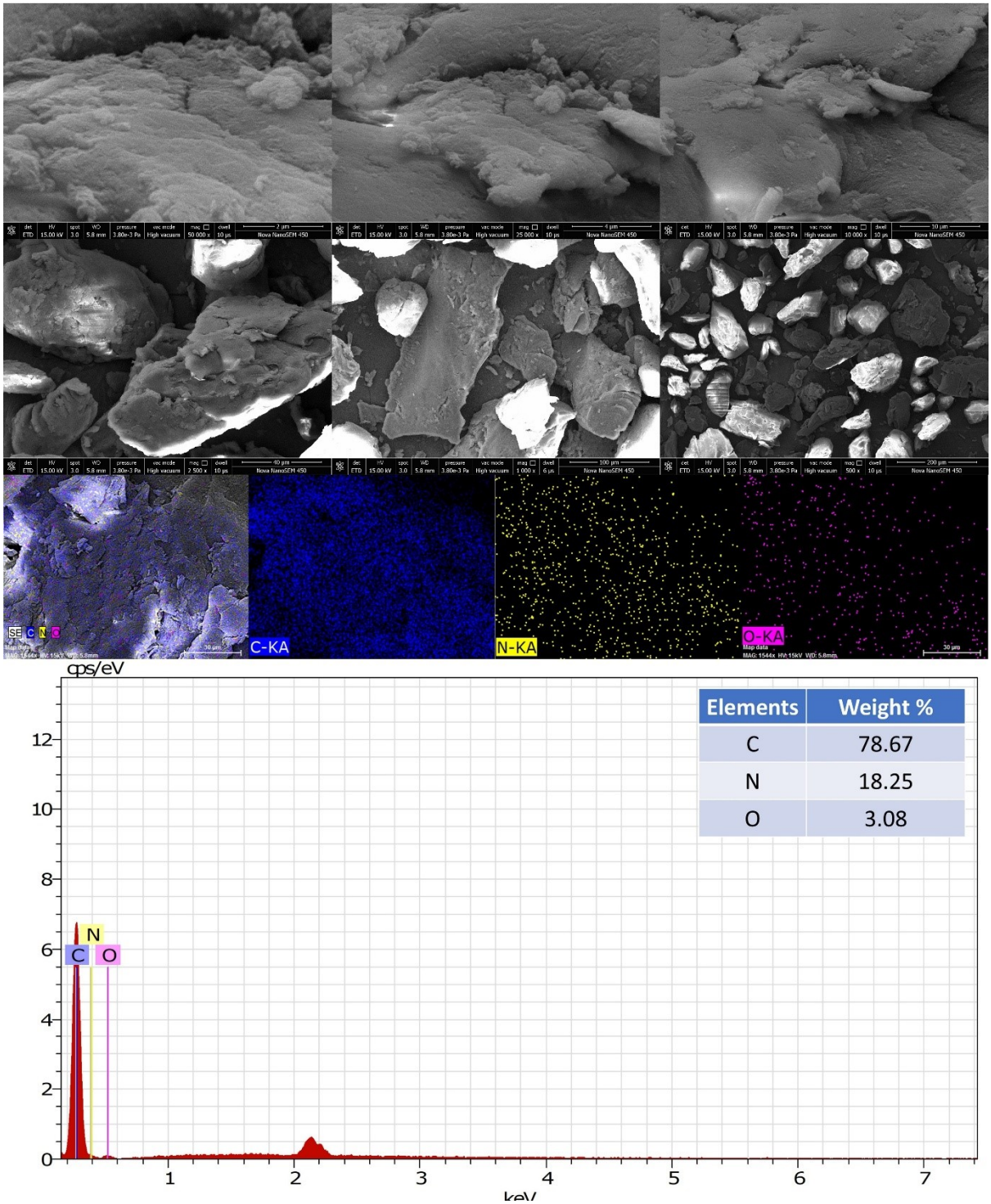

Figure S8. FE-SEM images of TBZTFPG-COP at different magnifications. Low-magnification images show irregular, plate-like particles with agglomeration, while high-magnification images reveal a rough, crumpled surface indicative of a layered 2D COP structure. Energy dispersive X-ray (EDX) mapping of TBZTFPG-COP in terms of constituent elements C, N and O. Elemental mapping and EDX analysis confirm the uniform elemental distribution within the framework.

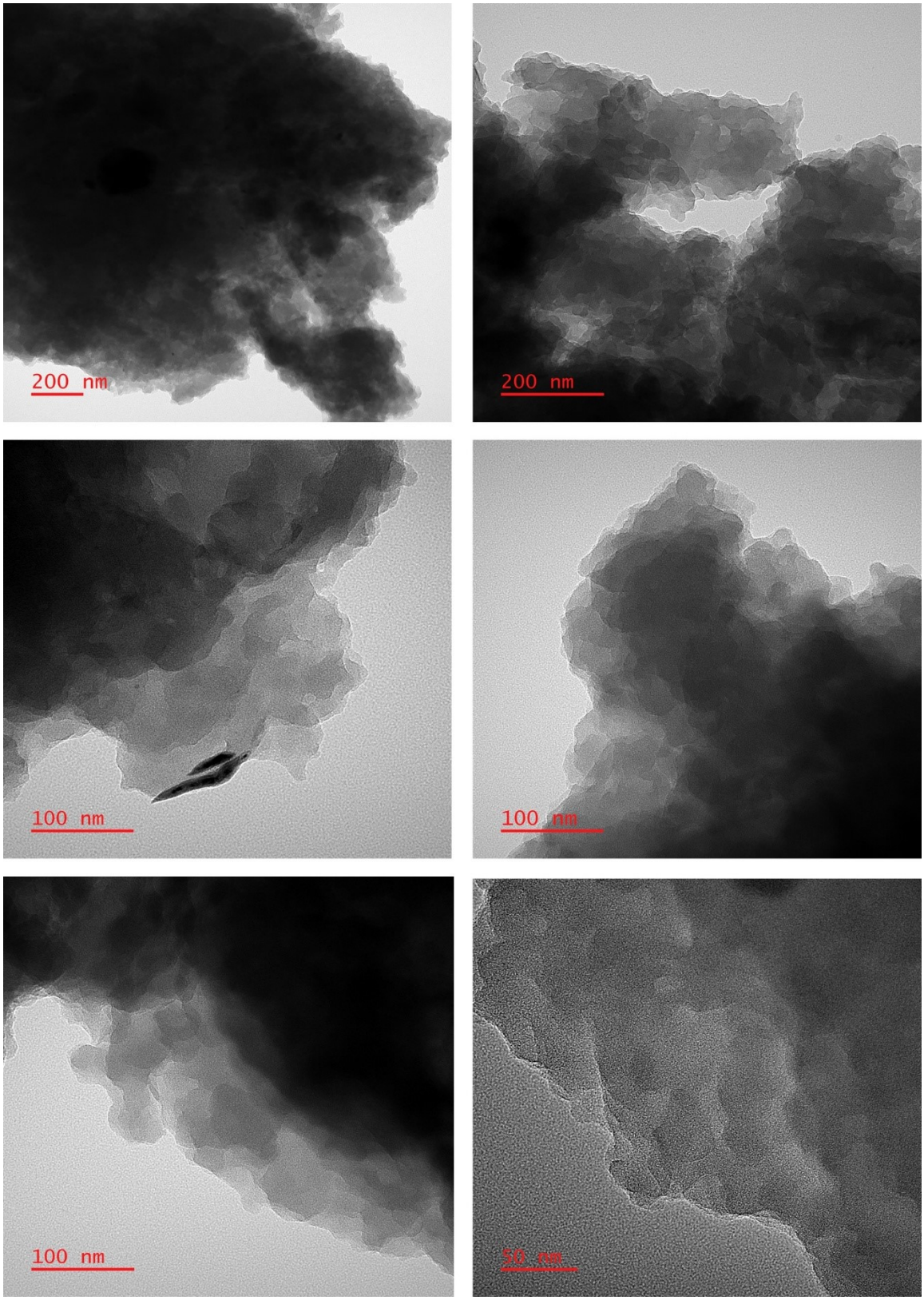

Figure S9. HR-TEM images of the TBZTFPG-COP under different magnifications showing the aggregates formed by stacking of many sheets. Darker regions are from such multi-flake stacking. While at 20 nm resolution the uniform micropores all along the surface of the COF can be seen.

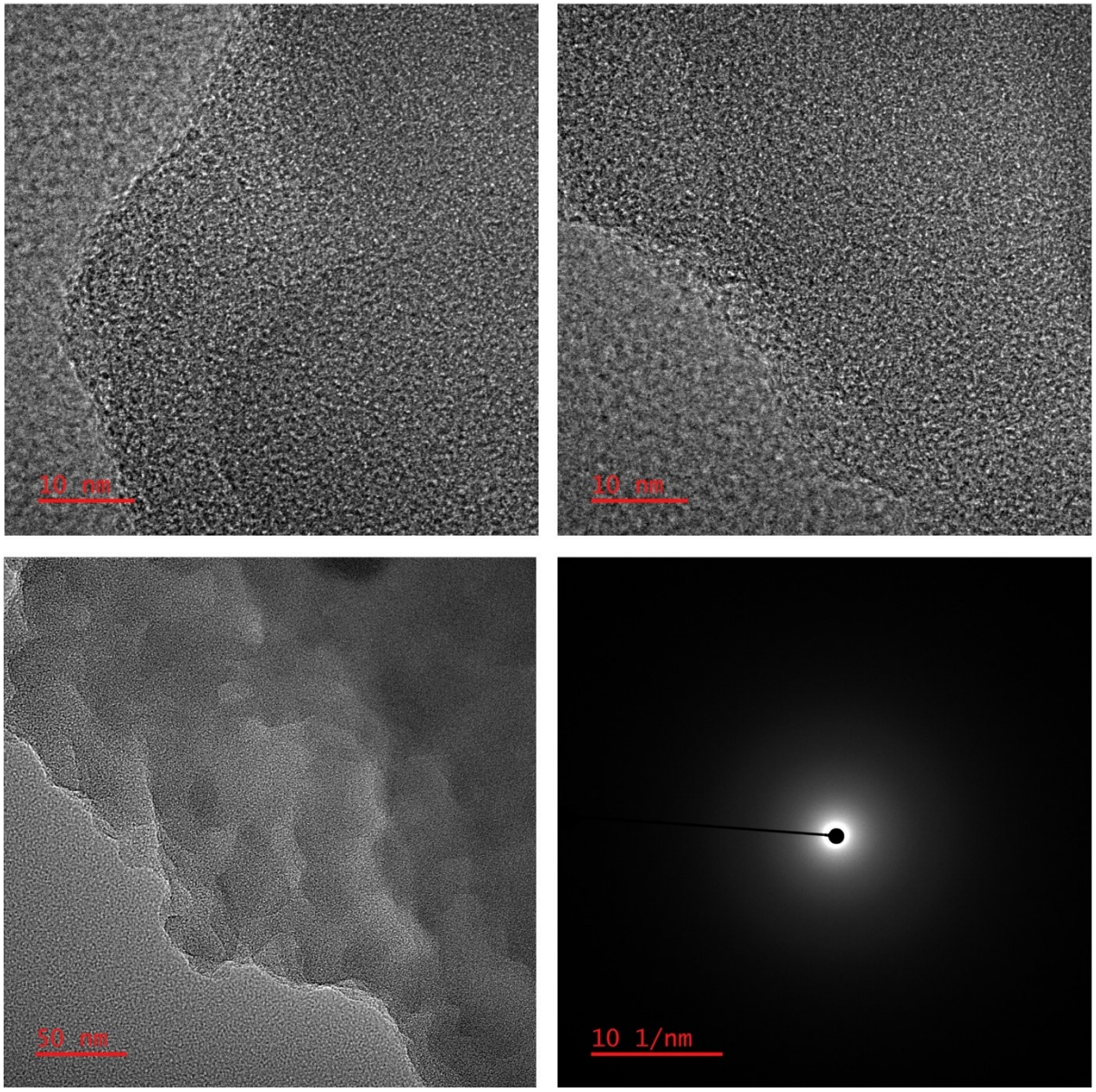

Figure S10. HR-TEM images of the TBZTFPG-COP under higher magnifications and SAED pattern of TBZTFPG-COP.

S6. CV Measurements

S6.1. Electrochemical characterization: Synthesized COP material was tested for Linear Sweep Voltammetry (LSV), Cyclic voltammetry (CV), Electrochemical Impedance Spectroscopy (EIS) and Galvanic Charge – Discharge (GCD) studies were performed using electrochemical workstation (Biologic, SP50e).

S6.2. Electrode preparation and supercapacitor fabrication: To examine the energy storage capabilities of the synthesized COP material, electrodes were prepared using stainless-steel sheet and electrochemical tests were performed using three-electrode, symmetric two-electrode and asymmetric two-electrode setups. In a three-electrode setup,

active material (TBZTFPG-COP) was mixed well with polyvinylidene fluoride (PVDF), and carbon black in the weight ratio of 8:1:1 and grinded well. Further, N-methyl-2-pyrrolidone solvent was added dropwise to the finely grinded mixture to make a slurry and this slurry was coated on the stainless-steel sheet of area 1cm^2 x 1cm^2 dimensions. The coated sheets were dried at 60-70 ºC under vacuum and further these sheets were used as working electrodes along with Ag/Agcl as a reference electrode and platinum foil as a counter electrode for the electrochemical evaluation. In a symmetric two-electrode system, two symmetrical stainless-steel sheets with the same above-mentioned dimensions were used as electrodes to fabricate a supercapacitor device. In an asymmetric two-electrode system, TBZTFPG-COP was used as a positive electrode and carbon black was used as a negative electrode to fabricate a supercapacitor device. All the electrochemical tests were performed using 1M H_2SO_4 electrolyte. The electrode active material loading on the stainless-steel substrate was 2 mg cm^{-2} in the three-electrode system and 4 mg cm^{-2} in the two-electrode system.

The specific capacitance was calculated using the following equation.

$$C_s\,(F\,g^{-1}) = \frac{A}{2km\Delta V}$$

Where, C_s is specific capacitance (F g^{-1}), A is current(A), k is scan rate (V/s), m is mass (g), and ΔV is potential window (V).

The energy density and power density for the supercapacitor devices were calculated using the following equation.

$$E_d\,(Wh\,kg^{-1}) = \frac{CV^2 \times 1000}{2 \times 3600}$$

where, E_d is Energy density, C is specific capacitance and V is operating voltage.

$$P_d\,(W\,kg^{-1}) = \frac{E_d \times 3600}{\Delta t}$$

where, P_d is the power density, E_d is the energy density and Δt is the time.

$$\Delta t = \frac{\Delta V}{S}$$

Where ΔV is Voltage Window, S is scan rate (V/s)

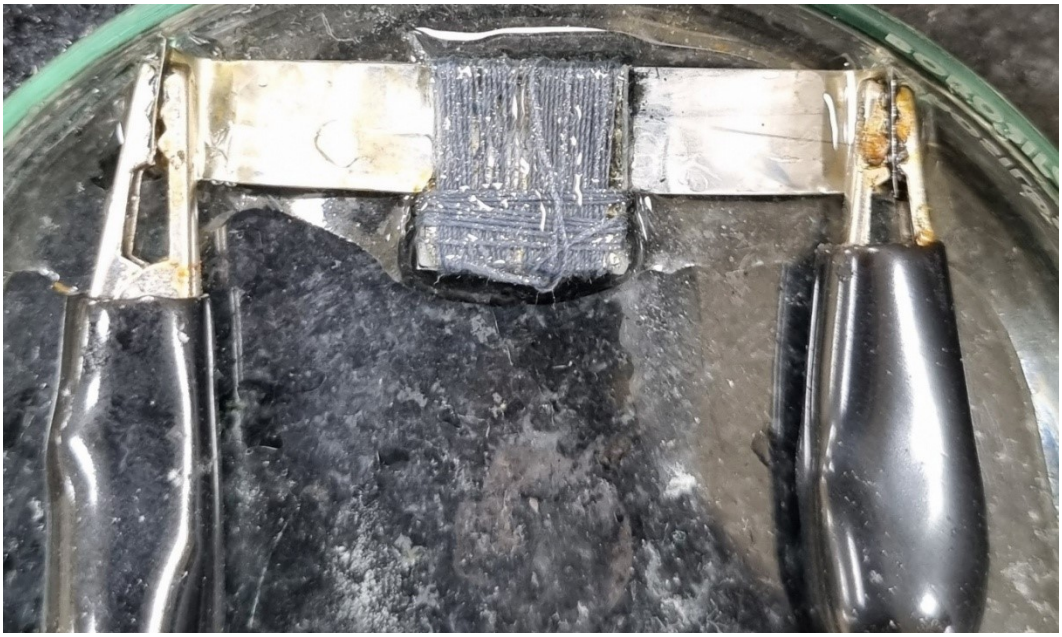

Figure S11. Image of the Supercapacitor device.

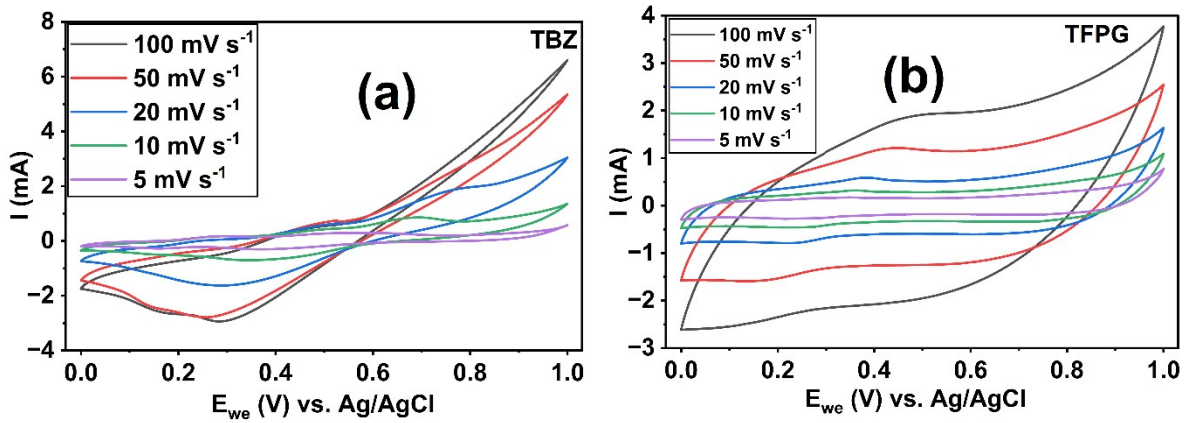

Figure S12. CV of the (a) TBZ monomer, (b) TFPG monomer at various scan rates.

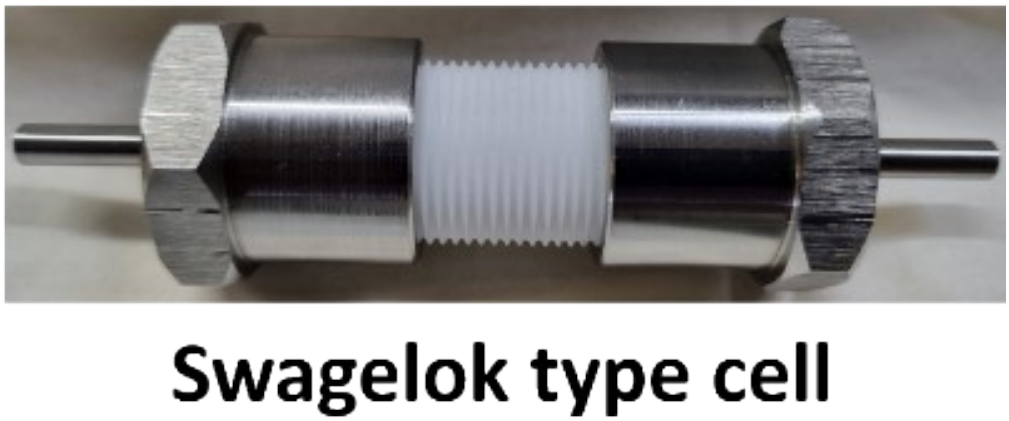

Figure S13. Photograph of the fabricated swagelok type supercapacitor device.

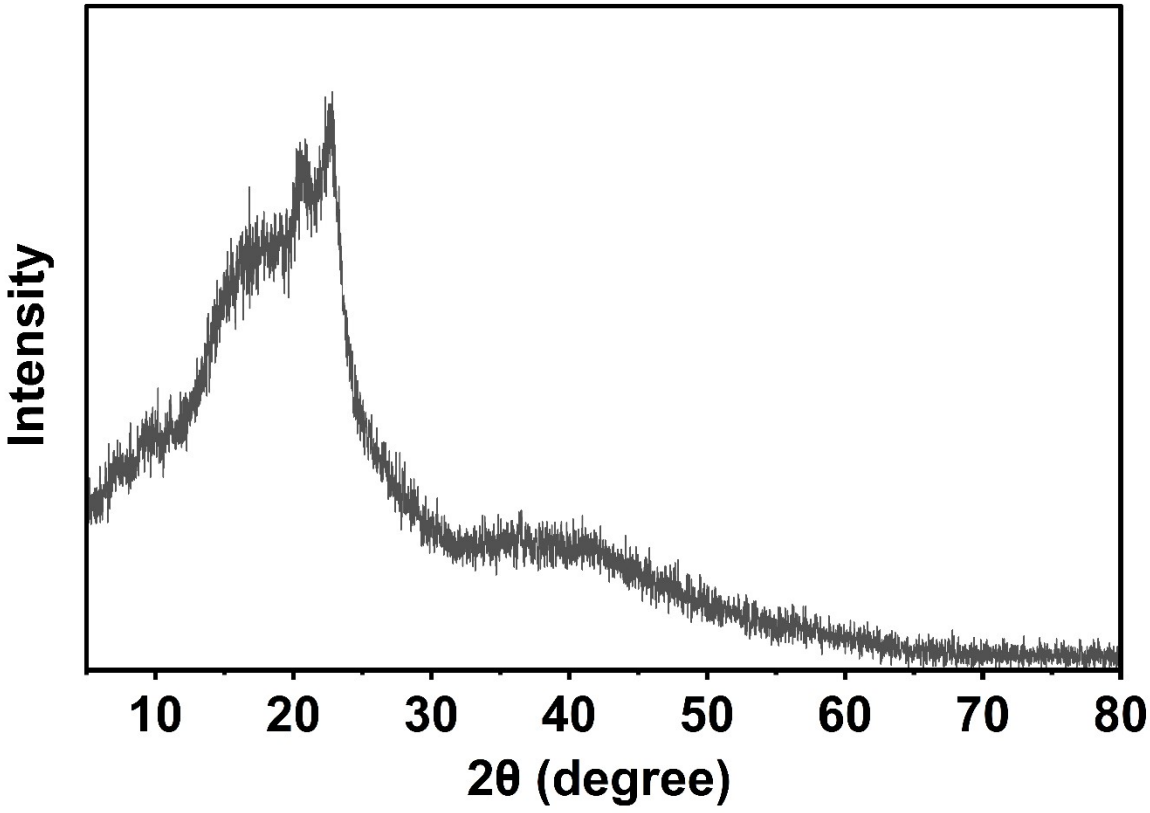

Figure S14. XRD plot of TBZTFPG-COP after cycling stability over 5000 cycles.

Table S2: Comparison of electrochemical performance of different polymer and framework materials as electrode materials for supercapacitors.

Materials	Surface area	Electrolyte	Three electrode setup		Two electrode setup		Number of cycles, Retention	References
			Csp	ED	Csp	ED and PD		
TPT-DAHQ COF	1855	0.1 M KOH	256 F/g	43 Wh/kg	-	-	1800, 81.5%	[3]
IISERP COF10	1233	1 M H_2SO_4/PVA	-	-	~92 mF/cm^2	98 μW/cm^2	10000, 83 %	[4]
IISERP COF11	921	1 M H_2SO_4/PVA	-	-	~32 mF/cm^2	~ 102 μW/cm^2	10000, 88 %	[4]
g-C34N6 COF	1003	LiCl/PVA	-	-	15.2 mF/cm^2	7.3 mWh/cm^3	5000, 93.1%	[5]
COF TDFP-1	651	0.1 M H_2SO_4	354 F/g	58 Wh/kg	-	-	1000, 95.0%	[6]
TPDA-COF	28.0	1 M Na_2SO_4	-	-	70.6 F/g	9.8 mW h/g	10000, 81.5%	[7]
TTT-DHTD COF	839	1 M KOH	273.3 F/g	-	-	-	2000, 99%	[8]
CAP-2	594	2M KCl	240 F/g	-	233 F/g	23 Wh/kg	10000,80%	[9]
DAAQ-TFP COF	-	1 M H_2SO_4	3 mF/cm^2	-	-	-	5000, ~93%	[10]
TaPaPy	687	1 M H_2SO_4	209 F/g	-	102 F/g	9.06 Wh/kg	6000,92%	[11]
POP-1	260	3 M KOH	192 F g^{-1}				10,000, 94%)	[12]
POP-2	342	3 M KOH	192 F g^{-1}				92(10,000@1)	[12]
CzT-CMOP-1	615	6 M KOH	240 F g^{-1}	-	-	-	2000, 97%	[13]

TAT-CMP-1	88	1 M Na_2SO_4	141 F g^{-1}	-	-	-	10000, 83%	[14]
TAT-CMP-2	106	1 M Na_2SO_4	183 F g^{-1}	-	-	-	10000, 95 %	[14]
TPT-CTFs	128.53	1 M H2SO4	110 F/g	-	13 F/g	4.2 Wh/kg and 250 W/kg	10000, 105 %	[15]
CTF-600	-	1 M KOH	458 F/g	-	16 F/g	8 Wh/kg and 250 W/kg	5000, 92.15%	[16]
PDC-MA-COF	748.2	6 M KOH aqueous solution	335 F/g	-	94 F/g	29.2 Wh/kg and 750 W/kg	20000, 88%	[17]
IITR-COF-1	2830	0.5 M K_2SO_4 (aq)	182.6 F/g	101.5 Wh/kg	30.7 F/g	17.0 Wh/kg and 119.3 W/kg	5000, 97.8%	[18]
COF/rGO hybrid	498	1M.H_2SO_4	321 F/g	-	74 F/g	10.3 Wh/kg and 50 W/kg	5000, 94.3%	[19]
TFPDQGO	267.5	1 M NaCl	429.0 F/g	-	118.5 F/g	59.4 Wh/kg and 950 W/kg	10000, 80.6%	[20]
Co_3S_4@$NiCo_2S_4$ (CS/NCZS)	-	6 M KOH	2697.7 F/g	-	224.2 F/g	79.7 Wh/kg and 693.5 W/kg	10000, 79.3%	[21]
COP (porphyrin-based COP wrapped on MWCNT)	-	5 M $NaClO_4$	292.7 F/g	196.8 Wh/kg and 752 W/kg	55.5 F/g	37.3 Wh/kg	20000, 100 %	[22]
TPTP-COF@f-CNF	-	6 M KOH	577.4 F/g	-	56.4 F/g	34.6 Wh/kg and 831 W/kg	10 000, 81.5 %	[23]
EG@COF-3	1397	6 M KOH	501 F/g	-	45 F/g	16.4 Wh/kg and 806 W/kg	10 000, 92.3 %	[24]
PANI/PEDOT/PSS @ PI-COF-	1080	0.5 M H_2SO_4	729.2 F/g	-	182 F/g	-	10 000, 89.8 %	[25]

700								
COP (FCF@PCOP-SO_3)	-	0.1 M H_2SO_4	670.8 F/g	21.9 Wh/kg abd 450 W/kg	-	-	10000, 96.4%	[26]
(HDC-PC)	612	3 M KOH	678 F/g	22.3 Wh/kg and 450 W/kg	312 F/g	21.5 Wh/kg and 520 W/kg	10000, 92%	[25]
TBZTFPG-COP	**281.93**	**1 M H_2SO_4**	**824 F/g**	**114.4 Wh /Kg and 10,000 W/kg**	**111.4 F/g**	**15.4 Wh/kg and 2500 W/kg**	**10000, 97% Columbic efficiency 96%**	**This work**

References

1. J. Liu, Y. Li, Y. Li and N. Hu, Ethylene polymerization by (α-diimine)nickel(II) complexes bearing different substituents on para-position of imines activated with MMAO, *Journal of Applied Polymer Science*, 2008, **109**, 700-707.
2. P. Wehrmann and S. Mecking, Highly Active Binuclear Neutral Nickel(II) Catalysts Affording High Molecular Weight Polyethylene, *Organometallics*, 2008, **27**, 1399-1408.
3. A. F. El-Mahdy, Y. H. Hung, T. H. Mansoure, H. H. Yu, T. Chen and S. W. Kuo, A hollow microtubular triazine-and benzobisoxazole-based covalent organic framework presenting sponge-like shells that functions as a high-performance supercapacitor, *Chemistry–An Asian Journal*, 2019, **14**, 1429-1435.
4. S. Haldar, R. Kushwaha, R. Maity and R. Vaidhyanathan, Pyridine-Rich Covalent Organic Frameworks as High-Performance Solid-State Supercapacitors, *ACS Materials Letters*, 2019, **1**, 490-497.
5. J. Xu, Y. He, S. Bi, M. Wang, P. Yang, D. Wu, J. Wang and F. Zhang, An olefin-linked covalent organic framework as a flexible thin-film electrode for a high-performance micro-supercapacitor, *Angewandte Chemie*, 2019, **131**, 12193-12197.
6. P. Bhanja, K. Bhunia, S. K. Das, D. Pradhan, R. Kimura, Y. Hijikata, S. Irle and A. Bhaumik, A New Triazine-Based Covalent Organic Framework for High-Performance Capacitive Energy Storage, *ChemSusChem*, 2017, **10**, 921-929.
7. H.-C. Yang, Y.-Y. Chen, S.-Y. Suen and R.-H. Lee, Triazine-based covalent organic framework/carbon nanotube fiber nanocomposites for high-performance supercapacitor electrodes, *Polymer*, 2023, **273**, 125853.
8. S. Li, B. Kumbhakar, B. Mishra, J. Roeser, N. Chaoui, J. Schmidt, A. Thomas and P. Pachfule, Dithiophenedione-Based Covalent Organic Frameworks for Supercapacitive Energy Storage, *ACS Applied Energy Materials*, 2023, **6**, 9256-9263.
9. W. Liu, M. Ulaganathan, I. Abdelwahab, X. Luo, Z. Chen, S. J. Rong Tan, X. Wang, Y. Liu, D. Geng, Y. Bao, J. Chen and K. P. Loh, Two-Dimensional Polymer Synthesized via Solid-State Polymerization for High-Performance Supercapacitors, *ACS Nano*, 2018, **12**, 852-860.
10. C. R. DeBlase, K. Hernández-Burgos, K. E. Silberstein, G. G. Rodríguez-Calero, R. P. Bisbey, H. D. Abruña and W. R. Dichtel, Rapid and Efficient Redox Processes within 2D Covalent Organic Framework Thin Films, *ACS Nano*, 2015, **9**, 3178-3183.
11. A. M. Khattak, Z. A. Ghazi, B. Liang, N. A. Khan, A. Iqbal, L. Li and Z. Tang, A redox-active 2D covalent organic framework with pyridine moieties capable of faradaic energy storage, *Journal of Materials Chemistry A*, 2016, **4**, 16312-16317.
12. T. Li, W. Zhu, R. Shen, H.-Y. Wang, W. Chen, S.-J. Hao, Y. Li, Z.-G. Gu and Z. Li, Three-dimensional conductive porous organic polymers based on tetrahedral polythiophene for high-performance supercapacitors, *New Journal of Chemistry*, 2018, **42**, 6247-6255.
13. A. F. M. El-Mahdy, J. Lüder, M. G. Kotp and S.-W. Kuo, A Tröger's Base-Derived Covalent Organic Polymer Containing Carbazole Units as a High-Performance Supercapacitor.*Journal*, 2021, **13**.
14. X.-C. Li, Y. Zhang, C.-Y. Wang, Y. Wan, W.-Y. Lai, H. Pang and W. Huang, Redox-active triazatruxene-based conjugated microporous polymers for high-performance supercapacitors, *Chemical Science*, 2017, **8**, 2959-2965.
15. S. Xiong, J. Guo, F. Lv, X. Zhao, W. Zhang, X. Wang, C. Hua, R. Zhang, J. Chu, C. Wang, M. Gong and B. Wu, Solvothermal synthesis and supercapacitive properties of highly electrochemical stable covalent organic frameworks with triazine building block, *Journal of Applied Polymer Science*, 2023, **140**, e54538.
16. X. Zhang, Z. Zhang, R. Xiong, X. Xu, X. Tian and C. Wang, High Temperature Modified Covalent Triazine Framework for High-efficiency and Ultra-cycle Stable Symmetric Supercapacitor, *Chemistry Letters*, 2022, **51**, 854-858.

17. L. Li, F. Lu, R. Xue, B. Ma, Q. Li, N. Wu, H. Liu, W. Yao, H. Guo and W. Yang, Ultrastable Triazine-Based Covalent Organic Framework with an Interlayer Hydrogen Bonding for Supercapacitor Applications, *ACS Applied Materials & Interfaces*, 2019, **11**, 26355-26363.
18. Y. Kumar, I. Ahmad, A. Rawat, R. K. Pandey, P. Mohanty and R. Pandey, Flexible Linker-Based Triazine-Functionalized 2D Covalent Organic Frameworks for Supercapacitor and Gas Sorption Applications, *ACS Applied Materials & Interfaces*, 2024, **16**, 11605-11616.
19. C. Wang, F. Liu, J. Chen, Z. Yuan, C. Liu, X. Zhang, M. Xu, L. Wei and Y. Chen, A graphene-covalent organic framework hybrid for high-performance supercapacitors, *Energy Storage Materials*, 2020, **32**, 448-457.
20. L. Xu, Y. Liu, Z. Ding, X. Xu, X. Liu, Z. Gong, J. Li, T. Lu and L. Pan, Solvent-Free Synthesis of Covalent Organic Framework/Graphene Nanohybrids: High-Performance Faradaic Cathodes for Supercapacitors and Hybrid Capacitive Deionization, *Small*, 2024, **20**, 2307843.
21. C. Ni, X. Wang, X. Cai, C. Yu, Q. Wu, Y. Shen and C. Hao, Construction of core-shell heterostructures Co3S4@NiCo2S4 as cathode and covalent organic framework derived carbon as anode for hybrid supercapacitors, *Journal of Materials Science & Technology*, 2025, **210**, 233-245.
22. M. Tasleem, I. Ahmad and M. Sankar, Porphyrin-Based Covalent Organic Polymer Wrapped MWCNT Electrodes under Moderate Salt Concentration for Super-Stable Aqueous Sodium-Ion Intercalated Sustainable Supercapacitor, *Small*, 2025, **21**, e2409580.
23. R. Xue, H. Gou, Y. Liu and H. Rao, A layered triazinyl-COF linked by− NH− linkage and resulting N-doped microporous carbons: preparation, characterization and application for supercapacitance, *Journal of Porous Materials*, 2021, **28**, 895-903.
24. J. Khan, A. Ahmed and A. A. Al-Kahtani, Enhanced supercapacitor performance using EG@COF: a layered porous composite, *RSC Advances*, 2025, **15**, 11441-11450.
25. A. Devendran and A. Nagai, Covalent organic framework-derived highly defective carbon-integrated polymer composite electrode for supercapacitor applications, *ACS Applied Energy Materials*, 2025, **8**, 2597-2611.
26. R. Azizi, M. Shamsipur, A. A. Taherpour, M. Miri and A. Pashabadi, 3D honeycomb porous sulfonated covalent organic polymer (PCOP) synthesized on carbon fabric at refrigerated temperature: supercapacitor and metal-free proton relay for water oxidation in alkaline and neutral media, *Materials Advances*, 2025, **6**, 6094-6108.